

Brownian motion of a charged colloid in restricted confinementYael Avni ^{1,2}, Shigeyuki Komura ², and David Andelman ¹¹*Raymond and Beverly Sackler School of Physics and Astronomy, Tel Aviv University, Ramat Aviv 69978, Tel Aviv, Israel*²*Department of Chemistry, Graduate School of Science, Tokyo Metropolitan University, Tokyo 192-0397, Japan*

(Received 13 December 2020; accepted 23 March 2021; published 19 April 2021)

We study the Brownian motion of a charged colloid, confined between two charged walls, for small separation between the colloid and the walls. The system is embedded in an ionic solution. The combined effect of electrostatic repulsion and reduced diffusion due to hydrodynamic forces results in a specific motion in the direction perpendicular to the confining walls. The apparent diffusion coefficient at short times as well as the diffusion characteristic time are shown to follow a sigmoid curve as a function of a dimensionless parameter. This parameter depends on the electrostatic properties and can be controlled by tuning the solution ionic strength. At low ionic strength, the colloid moves faster and is localized, while at high ionic strength it moves slower and explores a wider region between the walls, resulting in a larger diffusion characteristic time.

DOI: [10.1103/PhysRevE.103.042607](https://doi.org/10.1103/PhysRevE.103.042607)**I. INTRODUCTION**

Understanding the Brownian motion of colloids under confinement has been a great challenge in recent decades [1]. Such motion is present in the segregation and transport of particles through biocellular membranes [2], in microfluidic devices [3], and in particle trapping and tracking technologies [4,5].

A simple example of confinement is observed when a colloid is placed in a confined space bounded by rigid surfaces. In this case, the colloid motion differs from its free medium one (no boundaries) due to hydrodynamic forces between the colloid and the confining surfaces. At low Reynolds numbers, this effect reduces to a change in the drag coefficient, which in turn leads to a position-dependent diffusion coefficient (PDDC) of the colloid. For simple geometries such as a spherical colloid near a single planar wall or in between two flat walls, the PDDC was calculated by Brenner and co-workers [6,7] and Ganatos *et al.* [8,9]. These results were verified experimentally for micro- or nanometer-sized particles, by different techniques of light scattering [10–13], video microscopy [14], optical tweezers [15] and total internal reflection velocimetry [16].

In polar solvents, the colloid and the confining surfaces often carry an electric charge, and the interaction between them confines the colloid even further to the vicinity of some potential minimum [17]. This results in an intricate motion which is affected both by the PDDC and the confining potential.

Consequently, the colloid motion was examined experimentally in the lateral direction [18,19]. However, its motion in the direction perpendicular to the confining surfaces, where the coupling between the PDDC and the interaction potential is pronounced, was only examined when the diffusion coefficient does not change throughout the colloid motion [20,21]. Although this simplification is valid at times, a rigorous de-

scription of the motion in which the PDDC and interaction potential are fully coupled to one another is still missing. Moreover, in previous studies, the electrostatic interaction was approximated by the simplified form, $U \sim \exp(-d/\lambda_D)$, where λ_D is the Debye screening length and d is the separation distance between the surface of the colloid and the wall. While this is valid in the large separation limit $d \gg \lambda_D$, the interesting regime where d is of the order of λ_D has yet to be explored.

In this paper, we study the motion of a spherical charged colloid, of radius a , confined between two charged walls, and focus on the motion in the direction perpendicular to the walls. We consider the large sphere limit, i.e., $a \gg \lambda_D$, d , for which the calculation greatly simplifies and analytical results are obtained. We make an additional simplification by approximating the interaction potential to be a harmonic one around the equilibrium position. We obtain a dynamical equation that depends on a single dimensionless parameter, α , that quantifies the interplay between the walls and the interaction potential.

In the small or large α limits, the calculated probability distribution function agrees with previous results, while for $\alpha \sim 1$, the motion deviates substantially from these two known cases. The difference is quantified by the mean-square displacement (MSD) behavior as a function of time, where an analytic expression for the short-time behavior is derived, while the long-time behavior is studied numerically. We also show the dependence of α on the electrostatic properties of the system. In particular, we demonstrate how it can be tuned by changing the salt concentration, causing the colloid motion to cross over between the PDDC dominated motion, which is slow and explores a wide region, and the electrostatically dominated one, which is faster and more localized.

The outline of the paper is as follows. In Sec. II, we calculate the interaction potential. In Sec. III, we calculate the PDDC and derive the dynamical equation of the colloid

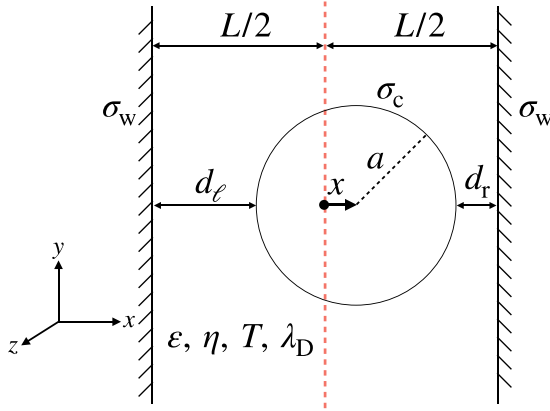


FIG. 1. Schematic drawing of the system. A colloid of surface charge density σ_c and radius a is positioned in between two walls with distance L between them, each having a surface charge density σ_w . Both the colloid and walls are embedded in an ionic solution with dielectric constant ϵ , viscosity η , temperature T , and screening length λ_D .

motion. In Sec. IV, we analyze the MSD of the motion for different values of the parameter α , and show the dependence of α on the electrostatic properties of the system. In Sec. V, we conclude with several general observations and comments on the validity of our results.

II. ELECTROSTATIC POTENTIAL

We consider a spherical colloid of radius a and charge Q , embedded in a dilute ionic solution. The charge of the colloid is assumed to be distributed homogeneously on its surface, with surface charge density $\sigma_c = Q/(4\pi a^2)$, where σ_c can be either positive or negative. The ionic solution is characterized by a dimensionless dielectric constant ϵ , viscosity η , temperature T , and bulk concentration of monovalent salt n . The colloid is confined between two charged walls, as shown in Fig. 1. The distance between the walls is L , and the position of the center of the colloid relative to the midplane between the two walls is x . The distance between the colloid and the left (right) wall is denoted by d_ℓ (d_r), such that $d_\ell = L/2 - a + x$ and $d_r = L/2 - a - x$. We define $d_0 = L/2 - a$ as the distance between the colloid and the walls when the colloid is placed on the midplane ($x = 0$). We also assume that the walls have a fixed charge density, σ_w , which can be either positive or negative.

The electrostatic interaction between a spherical colloid and a flat wall, embedded in an ionic solution, is described by the Poisson-Boltzmann theory [22,23]. Assuming that the colloid and wall are not highly charged [see the exact condition in Appendix A after Eq. (A2)], the theory can be linearized and reduces to the Debye-Hückel (DH) theory. In the DH theory, the electrostatic potential, ψ , at each point in space $\mathbf{r} = (x, y, z)$ is given by the linearized equation

$$(\nabla^2 - \kappa_D^2)\psi(\mathbf{r}) = 0, \quad (1)$$

where κ_D is the inverse screening length, $\kappa_D = \lambda_D^{-1} = [2e^2 n / (\epsilon_0 \epsilon k_B T)]^{1/2}$, λ_D is the Debye screening length, e is the elementary charge, ϵ_0 is the vacuum permittivity, and

k_B is the Boltzmann constant. The equation is solved together with the boundary conditions of fixed charge on the colloid surface and on the walls.

The DH equation does not have an analytic solution for the geometry considered here. However, by assuming that a is the largest length scale in the system, $a \gg d_\ell, d_r, \lambda_D$ (the large sphere limit), Eq. (1) can be solved by using the Derjaguin approximation. Note that the large sphere limit combines two different and independent physical limits: $a \gg d_\ell, d_r$ (narrow confinement) and $a \gg \lambda_D$ (thin double layer).

In Appendix A, we calculate the electrostatic potential ψ in the large sphere limit. In addition, the Appendix contains the detailed derivation of the interaction potential, $U(x)$, between the colloid and the charged walls, in the same limit. For convenience, we repeat here only the final expression relating $U(x)$ and the osmotic pressure, Π ,

$$U(x) = -2\pi a \left(\int^{d_0+x} dh \int_h^\infty dl \Pi(l) + \int^{d_0-x} dh \int_h^\infty dl \Pi(l) \right), \quad (2)$$

where the osmotic pressure, Π [23], is related to ψ by

$$\Pi = \frac{\epsilon \epsilon_0}{2} (-\psi'^2 + \kappa_D^2 \psi^2), \quad (3)$$

and ψ' is the first derivative along the x direction (note that $U(x)$ is defined up to a constant).

Equations (2) and (3) (see details in Appendix A) yield the following interaction potential:

$$U(x) = \frac{\pi a}{\epsilon \epsilon_0 \kappa_D^2} \left[2\sigma_c \sigma_w \ln \left(\frac{\cosh(\kappa_D d_0) + \cosh(\kappa_D x)}{\cosh(\kappa_D d_0) - \cosh(\kappa_D x)} \right) + (\sigma_c^2 + \sigma_w^2) \ln \left(\frac{\cosh(2\kappa_D d_0)}{\cosh(2\kappa_D d_0) - \cosh(2\kappa_D x)} \right) \right]. \quad (4)$$

Due to the symmetry, $U'(x) = 0$ at $x = 0$. However, from Eq. (4) it follows that this equilibrium is stable (minimum of U) only if

$$\frac{\sigma_w}{\sigma_c} < -e^{\kappa_D d_0} \quad \text{or} \quad \frac{\sigma_w}{\sigma_c} > -e^{-\kappa_D d_0}. \quad (5)$$

This is exactly the condition that the walls repel the colloid placed at the midplane position $x = 0$, instead of attracting it [24]. In what follows, we focus on the case where the colloid and walls have the same charge sign, and the stability condition, Eq. (5), is thus always satisfied.

Expanding $U(x)$ to second order around the midplane, $x = 0$, we obtain the harmonic potential approximation

$$U \approx \frac{1}{2} K x^2, \quad (6)$$

where $K = U''|_{x=0}$ is the effective spring constant. From Eq. (4), this approximation leads to

$$K = \left(\frac{2\pi a}{\epsilon_0 \epsilon} \right) \frac{2\sigma_c \sigma_w \cosh(\kappa_D d_0) + \sigma_c^2 + \sigma_w^2}{\sinh^2(\kappa_D d_0)}. \quad (7)$$

The harmonic interaction potential in Eq. (6) will be used as the potential energy in the following analysis. The approximation underestimates the strength of the interaction potential

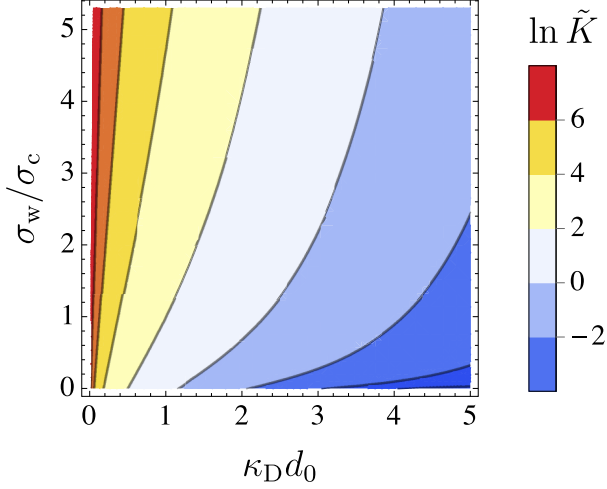


FIG. 2. Contour plot of the normalized effective spring constant, $\tilde{K} \equiv K/(\pi a \sigma_c^2/\epsilon_0 \epsilon)$ where $K = U''(x)|_{x=0}$ [see Eqs. (6) and (7)] as a function of $\kappa_D d_0$ and σ_w/σ_c . The color code is associated with $\ln \tilde{K}$. Large \tilde{K} is obtained in the high σ_w/σ_c and small $\kappa_D d_0$ limits. It decays to zero as $\kappa_D d_0$ is increased.

close to the walls, but this only has a minor effect on the dynamics, as will be discussed in depth in Sec. V.

In Fig. 2, $\tilde{K} \equiv K/(\pi a \sigma_c^2/\epsilon_0 \epsilon)$ is plotted for different $\kappa_D d_0$ and $\sigma_w/\sigma_c > 0$ values. For fixed $\kappa_D d_0$ and σ_c , K diverges as $\sigma_w \rightarrow \infty$, and monotonically decreases as σ_w decreases. For given σ_c and σ_w , K decreases rapidly when $\kappa_D d_0$ is increased.

In Appendix B we derive the corresponding K for fixed surface potential on the walls, rather than fixed surface charge.

III. CONFINED BROWNIAN DYNAMICS

A. Position-dependent diffusion coefficient (PDDC)

In a free medium (no boundaries), the colloid performs a simple Brownian motion, described by a diffusion coefficient D . By the Einstein relation, we have $D = \mu k_B T$, where μ is the mobility, defined by the ratio of the colloid terminal drift velocity to an applied force, $\mu = v/F$. If the colloid is neutral, and at low Reynolds number, the mobility follows the Stokes' law, $\mu = 1/(6\pi\eta a)$, and the diffusion coefficient of this motion is denoted as $D_\infty = k_B T/(6\pi\eta a)$.

The mobility of a charged colloid in an ionic solution is reduced due to the drag of the surrounding ionic cloud. However, for low surface electrostatic potential or low surface charge, the reduction is only of a few percent [25,26], and is therefore neglected here. Note that the motion of ions, by virtue of their small size, is much faster than the colloid, and is assumed to be in equilibrium throughout the colloid motion. Their only effect on the colloid dynamics (apart from the reduction of its mobility, which we neglect) is through the equilibrium interaction potential, Eq. (6).

The presence of walls in the vicinity of the colloid, however, can modify the colloid mobility substantially due to hydrodynamic effects. As shown by Brenner [6], the Stokes' law of a motion in the perpendicular direction to a single solid wall, at distance d , is modified in the following way:

$$F_\perp = 6\pi\eta a \lambda(\zeta) v_\perp, \quad (8)$$

with λ being

$$\lambda(\zeta) = \frac{4}{3} \sinh \zeta \sum_{n=1}^{\infty} \frac{n(n+1)}{(2n-1)(2n+3)} \times \left[\frac{2 \sinh[(2n+1)\zeta] + (2n+1) \sinh(2\zeta)}{4 \sinh^2[(n+1/2)\zeta] - (2n+1)^2 \sinh^2 \zeta} - 1 \right]. \quad (9)$$

Here $\zeta = \cosh^{-1}(1 + d/a)$, and F_\perp and v_\perp are the force and velocity in the perpendicular direction, respectively. In the $d \gg a$ limit, we have $\lambda = 1$ and the regular Stokes' law is recovered. In the $d \ll a$ limit, which is our main interest, Eq. (9) becomes, to leading order, $\lambda \approx a/d$.

When the colloid is placed in between two walls, the modified Stokes' law has a much more complicated expression, relying on extensive numerical computations [8]. However, several approximations have been proposed [11,27,28]. The simplest one is the linear superposition approximation that was shown to agree fairly well with experiments [29],

$$F_\perp \approx 6\pi\eta a (\lambda_\ell + \lambda_r - 1) v_\perp, \quad (10)$$

where λ_ℓ and λ_r are calculated from Eq. (9), with $d = d_\ell$ and $d = d_r$, respectively. Note that the negative third term in Eq. (10) guarantees that we recover $F_\perp = 6\pi\eta a v_\perp$ when the walls are very far apart.

In the narrow confinement limit, $d_\ell, d_r \ll a$, the perpendicular diffusion coefficient D_\perp can be approximated as

$$D_\perp(x) \approx D_\infty \frac{d_\ell d_r}{a(d_\ell + d_r)} = D_0 \left(1 - \frac{x^2}{d_0^2} \right), \quad (11)$$

where

$$D_0 = \frac{D_\infty d_0}{2a} \quad (12)$$

and the relations $d_\ell = d_0 + x$ and $d_r = d_0 - x$ were used. In Fig. 3, we compare between the approximated diffusion coefficient given by Eq. (11), and the “exact” numerical results of the diffusion coefficient of a colloid between two walls, for motion in the perpendicular direction. The numerical data is adapted from Fig. 6 of Ref. [8]. Here we show D_\perp/D_∞ , which is the inverse of λ , $D_\perp/D_\infty = 1/\lambda$, whereas in Ref. [8], λ was calculated [see its definition in Eq. (8)].

As seen in Fig. 3, for $L/(2a) = 1.5$, the approximated expression overestimates the “exact” one by $\sim 20\%$ at the midplane ($x = 0$), and becomes more accurate as we look away from the midplane. For $L/(2a) = 1.25$, the deviation in the midplane is of $\sim 10\%$, and decreasing away from the midplane. For $L/(2a) = 1.1$, there is only one data point available at the midplane, and it deviates from the approximation by only $\sim 2\%$. This strongly supports that in the $d_0 \ll a$ limit ($L \approx 2a$), the approximated Eq. (11) can be used.

The parallel motion is also described by a position-dependent diffusion coefficient $D_\parallel(x)$ although we do not calculate it here [9].

B. Fokker-Planck equation

The dynamics of a colloid with diffusion coefficients $D_\perp(x)$ and $D_\parallel(x)$ in the perpendicular and parallel directions,

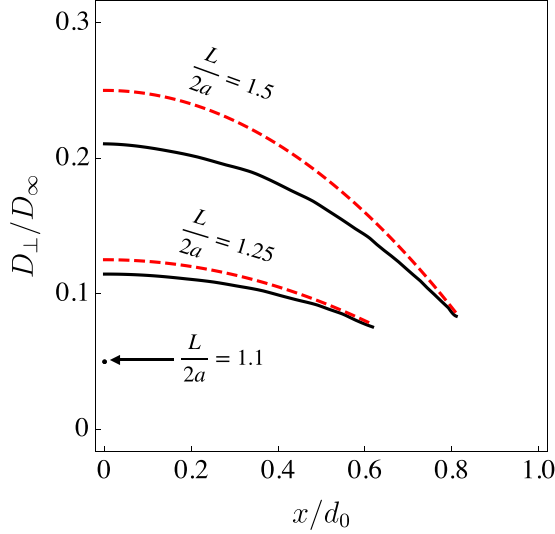


FIG. 3. The diffusion coefficient D_{\perp} of a colloid between two flat surfaces, normalized by its diffusion coefficient in a free medium, $D_{\infty} = k_B T / (6\pi\eta a)$, as a function of x/d_0 . Full black lines are numerical results obtained in Ref. [8], and red dashed lines show the approximated expression in Eq. (11), which relies on the linear superposition approximation in the $d_e, d_r \ll a$ limit. For $L/(2a) = 1.1$, a single data point was available in the numerical calculation: $D_{\perp}/D_{\infty} = 0.049$ at $x = 0$. The approximated expression in Eq. (11) yields $D_{\perp}/D_{\infty}(x = 0) = 0.05$ at $x = 0$. The difference between the two values is smaller than the plot resolution.

respectively, and under potential field $U(x)$, is governed by the generalized Fokker-Planck equation [30],

$$\frac{\partial P(\mathbf{r}, t)}{\partial t} = \frac{\partial}{\partial x} \left[D_{\perp}(x) \left(\frac{1}{k_B T} \frac{\partial U}{\partial x} + \frac{\partial}{\partial x} \right) P(\mathbf{r}, t) \right] + D_{\parallel}(x) \left(\frac{\partial^2}{\partial y^2} + \frac{\partial^2}{\partial z^2} \right) P(\mathbf{r}, t), \quad (13)$$

where $P(\mathbf{r}, t)$ is the time-dependent probability distribution function (PDF) of the colloid position. The full three-dimensional motion of the colloid is quite complex, because the motion in the y - z plane is coupled to the motion along the x axis through the diffusion coefficient $D_{\parallel}(x)$. However, our focus is on the perpendicular motion in the x direction, which by symmetry, does not depend on the position in the y - z plane. Then one can integrate the equation both over y and z from $-\infty$ to ∞ , and obtain

$$\frac{\partial p(x, t)}{\partial t} = \frac{\partial}{\partial x} \left[D_{\perp}(x) \left(\frac{1}{k_B T} \frac{\partial U}{\partial x} + \frac{\partial}{\partial x} \right) p(x, t) \right], \quad (14)$$

where $p(x, t)$ is the reduced probability distribution function $p(x, t) = \int dy dz P(\mathbf{r}, t)$.

Substituting the harmonic interaction potential obtained in Eq. (6) and the PDDC of Eq. (11), we obtain

$$\frac{\partial p}{\partial t} = D_0 \frac{\partial}{\partial x} \left[\left(1 - \frac{x^2}{d_0^2} \right) \left(\frac{Kx}{k_B T} p + \frac{\partial p}{\partial x} \right) \right]. \quad (15)$$

All the electrostatic effects are captured by the term proportional to K . We note that, in general, rigid walls impose zero current boundary conditions, i.e., $j = 0$ on the

walls, where the current is defined by the continuity equation $\partial p / \partial t = -\partial j / \partial x$. From Eq. (14), the current becomes $j = -D_{\perp}(x) [(Kx/k_B T) p + \partial p / \partial x]$. Notice that the conditions $j = 0$ at the walls are automatically satisfied by the fact that D_{\perp} vanishes there.

IV. MEAN-SQUARE DISPLACEMENT

Equation (15), together with the definitions of K and D_0 in Eqs. (7) and (12), respectively, is the principal equation of this paper. By solving it, one can derive the MSD, which can be measured in experiments. The MSD of an ensemble of colloids in equilibrium is

$$\langle (x(t) - x_0)^2 \rangle = \int_{-d_0}^{d_0} dx_0 \int_{-d_0}^{d_0} dx (x(t) - x_0)^2 p(x, x_0; t), \quad (16)$$

where $p(x, x_0; t)$ is the probability of a colloid to be at x_0 at time $t = 0$ and at x at time t . As the initial position, x_0 , is drawn from an equilibrium distribution, we can write $p(x, x_0; t)$ in terms of the conditional probability, $p(x, x_0; t) = p(x, t | x_0, 0) p_{\text{eq}}(x_0)$, where $p_{\text{eq}}(x_0) \propto \exp(-Kx_0^2/2k_B T)$. It then follows that the MSD is

$$\langle (x(t) - x_0)^2 \rangle = \frac{\int_{-d_0}^{d_0} dx_0 e^{-Kx_0^2/2k_B T} \langle (x(t) - x_0)^2 \rangle_{x_0}}{\int_{-d_0}^{d_0} dx_0 e^{-Kx_0^2/2k_B T}}. \quad (17)$$

where $\langle \mathcal{O} \rangle_{x_0}$ is the average over an ensemble of colloids with the same initial position, x_0 , at $t = 0$, i.e., $\langle \mathcal{O} \rangle_{x_0} = \int dx p(x, t | x_0, 0) \mathcal{O}$, with $p(x, t | x_0, 0)$ being a solution of Eq. (15) with the initial condition $p(x, 0) = \delta(x - x_0)$. The MSD resulting from Eq. (15) will be analyzed in depth in what follows.

A. Vanishing interaction potential limit

While Eq. (15) does not have an analytic solution, it can be solved for certain limits. In the *vanishing interaction potential limit*, K is omitted altogether and we are left with

$$\frac{\partial p}{\partial t} = D_0 \left[-\frac{2x}{d_0^2} \frac{\partial p}{\partial x} + \left(1 - \frac{x^2}{d_0^2} \right) \frac{\partial^2 p}{\partial x^2} \right]. \quad (18)$$

The above equation, for a colloid at $x = x_0$ at time $t = 0$, has the solution [30]

$$p(x, t | x_0, 0) = \frac{1}{2d_0} \sum_{n=0}^{\infty} (2n+1) e^{-D_0 n(n+1)t/d_0^2} \times P_n \left(\frac{x_0}{d_0} \right) P_n \left(\frac{x}{d_0} \right), \quad (19)$$

where $P_n(x)$ is the Legendre polynomial of order n . The PDF of Eq. (19) is characterized by the following first and second moments,

$$\begin{aligned} \langle x(t) \rangle_{x_0} &= x_0 e^{-2D_0 t/d_0^2}, \\ \langle x^2(t) \rangle_{x_0} &= x_0^2 e^{-6D_0 t/d_0^2} + \frac{d_0^2}{3} (1 - e^{-6D_0 t/d_0^2}), \end{aligned} \quad (20)$$

In the limit of $t \rightarrow \infty$, the PDF reduces to a uniform distribution between the two walls that are positioned at $x = \pm d_0$.

In the vanishing interaction-potential limit, $K = 0$, Eq. (17) simply becomes

$$\langle (x(t) - x_0)^2 \rangle = \frac{1}{2d_0} \int_{-d_0}^{d_0} dx_0 [\langle x^2(t) \rangle_{x_0} - 2x_0 \langle x(t) \rangle_{x_0} + x_0^2], \quad (21)$$

leading to the MSD

$$\langle (x(t) - x_0)^2 \rangle = \frac{2d_0^2}{3} (1 - e^{-2D_0 t/d_0^2}). \quad (22)$$

The above MSD approaches $2d_0^2/3$ in the limit of $t \rightarrow \infty$.

B. Strong interaction-potential limit

In the opposite *strong interaction-potential limit*, the confinement due to electrostatic effects is strong, and the colloid remains close to the midplane. Consequently, its diffusion coefficient does not change, and equals to D_0 . Then the term that depends on d_0 in Eq. (15) can be omitted, and we obtain

$$\frac{\partial p}{\partial t} = D_0 \left[\frac{K}{k_B T} \left(p + x \frac{\partial p}{\partial x} \right) + \frac{\partial^2 p}{\partial x^2} \right]. \quad (23)$$

Note that this is equivalent to the case of permeable walls, where the walls interact electrostatically but not hydrodynamically. Additionally, note that a strong interaction potential U does not contradict the assumption employed in Sec. II of a small electrostatic potential ψ . This is evident, for example, by the dependence of U on the colloid size [see Eq. (4)], which is absent in ψ [see Eq. (A2)].

The above equation can be solved for a colloid at $x = x_0$ at time $t = 0$, yielding [31]

$$p(x, t|x_0, 0) = \left(\frac{K}{2\pi k_B T (1 - e^{-2D_0 K t/k_B T})} \right)^{1/2} \times \exp \left[-\frac{K(x - x_0 e^{-D_0 K t/k_B T})^2}{2k_B T (1 - e^{-2D_0 K t/k_B T})} \right]. \quad (24)$$

For the averages, we can extend the integral range in $\langle \mathcal{O} \rangle_{x_0} = \int dx p(x, t|x_0, 0) \mathcal{O}$ from $\pm d_0$ to $\pm \infty$. Then the first and second moments are

$$\begin{aligned} \langle x(t) \rangle_{x_0} &= x_0 e^{-D_0 K t/k_B T}, \\ \langle x^2(t) \rangle_{x_0} &= x_0^2 e^{-2D_0 K t/k_B T} + \frac{k_B T}{K} (1 - e^{-2D_0 K t/k_B T}). \end{aligned} \quad (25)$$

For the MSD, Eq. (17) now reads

$$\begin{aligned} \langle (x(t) - x_0)^2 \rangle &= \left(\frac{K}{2\pi k_B T} \right)^{1/2} \int_{-\infty}^{\infty} dx_0 e^{-Kx_0^2/2k_B T} \\ &\times [\langle x^2(t) \rangle_{x_0} - 2x_0 \langle x(t) \rangle_{x_0} + x_0^2], \end{aligned} \quad (26)$$

yielding

$$\langle (x(t) - x_0)^2 \rangle = \frac{2k_B T}{K} (1 - e^{-D_0 K t/k_B T}), \quad (27)$$

which asymptotically approaches $2k_B T/K$ for $t \rightarrow \infty$. Equations (19) and (24) and their corresponding MSD functions, Eqs. (22) and (27), represent the two limiting dynamical behaviors.

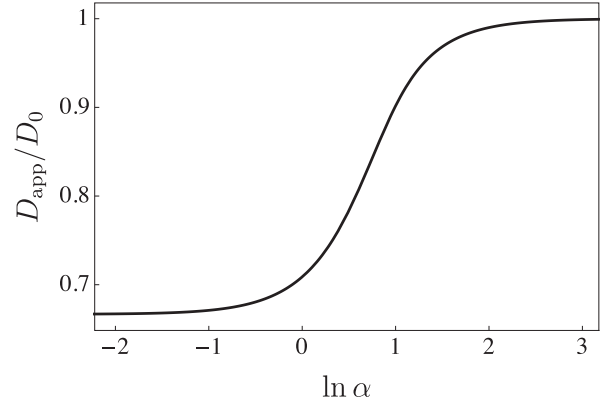


FIG. 4. The apparent diffusion coefficient D_{app} [see Eq. (30)], scaled by D_0 , as a function of $\alpha = Kd_0^2/k_B T$.

C. Short-time diffusion coefficient

For a known initial position, $p(x, 0)$ is infinitely sharp (Dirac delta function). As a result, the term proportional to the second derivative of p in Eq. (15) dominates the dynamics for short times,

$$\frac{\partial p}{\partial t} = D_{\text{eff}}(x_0) \frac{\partial^2 p}{\partial x^2}, \quad (28)$$

with $D_{\text{eff}}(x_0) \equiv D_0(1 - x_0^2/d_0^2)$. The colloid experiences, for a short while, a free diffusion with diffusion coefficient $D_{\text{eff}}(x)$, with the following conditional probability distribution function:

$$p(x, t|x_0, 0) = \left(\frac{1}{4\pi D_{\text{eff}}(x_0)t} \right)^{1/2} \exp \left[-\frac{(x - x_0)^2}{4D_{\text{eff}}(x_0)t} \right]. \quad (29)$$

This results in a linear time dependence of MSD, $\langle (x - x_0)^2 \rangle = 2D_{\text{app}}t$, where D_{app} is the apparent diffusion coefficient

$$\begin{aligned} D_{\text{app}} &= \frac{\int_{-d_0}^{d_0} dx_0 e^{-Kx_0^2/2k_B T} D_{\text{eff}}(x_0)}{\int_{-d_0}^{d_0} dx_0 e^{-Kx_0^2/2k_B T}} \\ &= D_0 \left[1 - \frac{1}{\alpha} + \frac{\sqrt{2/(\pi\alpha)} e^{-\alpha/2}}{\text{erf}(\sqrt{\alpha/2})} \right], \end{aligned} \quad (30)$$

where α is a dimensionless parameter defined by

$$\alpha = \frac{Kd_0^2}{k_B T} \quad (31)$$

and $\text{erf}(x) = (2/\sqrt{\pi}) \int_0^x e^{-z^2} dz$ is the error function. Notice that $\sqrt{\alpha}$ is the ratio between two characteristic length scales, d_0 and $\sqrt{k_B T/K}$. While d_0 is the length over which the diffusion coefficient changes, $\sqrt{k_B T/K}$ is the characteristic interaction potential length scale, which is small for strong potentials and large for weak ones.

In Fig. 4, D_{app}/D_0 is plotted as a function of α . Upon increasing α , D_{app} monotonically grows from $D_{\text{app}}/D_0 = 2/3$ obtained for $\alpha = 0$ to $D_{\text{app}}/D_0 = 1$ valid for the $\alpha \rightarrow \infty$ limit. We conclude that the colloid moves faster as the electrostatic effects are stronger (large α). The change in D_{app} occurs when α is of order unity.

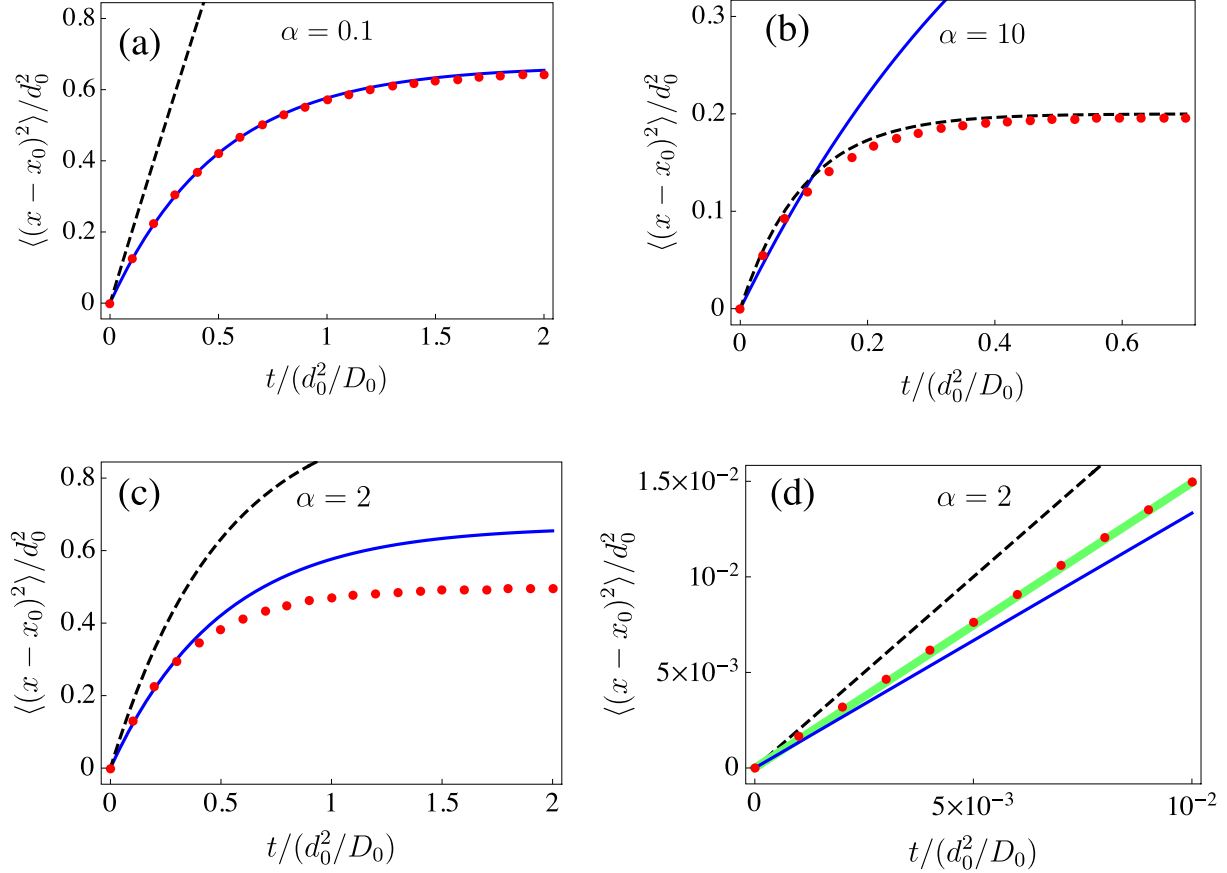


FIG. 5. The mean-square displacement (MSD) of the colloid, $\langle (x - x_0)^2 \rangle$ scaled by d_0^2 , as a function of t scaled by d_0^2/D_0 for (a) $\alpha = 0.1$, (b) $\alpha = 10$, and (c) and (d) $\alpha = 2$. Red dots are the numerical solution of Eq. (15). Solid blue line is the vanishing interaction-potential limit [see Eq. (22)]. Dashed black line is the strong interaction-potential limit [see Eq. (27)]. In (d), the short-time limit of $\alpha = 2$ is shown, together with the prediction, $\langle (x - x_0)^2 \rangle = 2D_{\text{app}}t$ with D_{app} defined in Eq. (30) (thick green line).

D. Numerical analysis

The full dynamical equation, Eq. (15), can be made dimensionless by using the dimensionless position $\tilde{x} = x/d_0$ and time $\tilde{t} = (D_0/d_0^2)t$ as

$$\frac{\partial p}{\partial \tilde{t}} = \frac{\partial}{\partial \tilde{x}} (1 - \tilde{x}^2) \left(\alpha \tilde{x} p + \frac{\partial p}{\partial \tilde{x}} \right), \quad (32)$$

where α is given by Eq. (31). The vanishing interaction-potential limit, Eq. (18), and strong interaction-potential limit, Eq. (23), correspond to $\alpha = 0$ and to the limit $\alpha \rightarrow \infty$, respectively [in order to obtain Eq. (23) from Eq. (32), one needs to redefine the normalized position and time].

We calculate the MSD of the particle for different α values by solving Eq. (32) numerically. In the following we use the same normalized variables as in Eq. (32), but drop the tilde signs for brevity. We divide our space into N lattice points $\{x_1, \dots, x_N\}$, where $x_1 = -1$ and $x_N = 1$, and define $p_i(t) \equiv p(x_i, t)$. For a given x_0 , we start with a distribution that approximates a Dirac delta function, $p_i(0) = (2\pi\delta)^{-1/2} \exp[(x_i - x_0)^2/2\delta]$, with $\delta \ll 1$. We then iterate each time step using

the Euler method,

$$\begin{aligned} p_i(t + \Delta t) &= p_i(t) + \frac{\Delta t}{\Delta x} \left[(1 - x_{i+1}^2) \left(\alpha x_{i+1} p_{i+1}(t) + \frac{p_{i+1}(t) - p_i(t)}{\Delta x} \right) \right. \\ &\quad \left. - (1 - x_i^2) \left(\alpha x_i p_i(t) + \frac{p_i(t) - p_{i-1}(t)}{\Delta x} \right) \right]. \end{aligned} \quad (33)$$

The zero current boundary condition is guaranteed due to the cancellation of the diffusion coefficient, proportional to $(1 - x_i^2)$, at x_1 and x_N . We used a lattice spacing of $\Delta x = 0.02$, and a time step Δt between 6.25×10^{-5} and 2×10^{-4} , depending on α . For each initial condition, $x_0 \in \{-1, 1\}$, we calculated $\langle (x(t) - x_0)^2 \rangle_{x_0}$ and obtained the MSD through Eq. (17).

The numerically obtained full MSD is shown in Fig. 5 for different α values, and is compared with the limits in Eqs. (22) and (27). Figure 5(a) shows that for $\alpha = 0.1$, the MSD coincides, almost perfectly, with the vanishing interaction potential case (solid blue line), while in Fig. 5(b) for $\alpha = 10$, it coincides with the strong interaction-potential case (dashed black line). However, for an intermediate value, $\alpha = 2$ in Fig. 5(c), the numerically obtained MSD deviates substantially from the

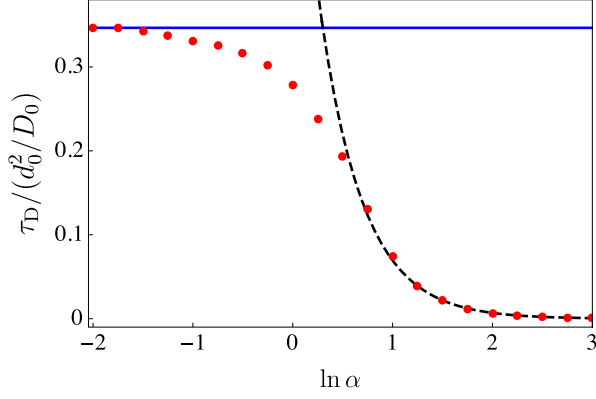


FIG. 6. The diffusion characteristic time τ_D , defined as the time at which the MSD reaches half of its value in the $t \rightarrow \infty$ limit, normalized by d_0^2/D_0 , as a function of α . Solid blue line is the vanishing interaction-potential limit, $\tau_D = d_0^2 \ln 2/(2D_0)$, and dashed black line is the strong interaction-potential walls limit, $\tau_D = d_0^2 \ln 2/(D_0\alpha)$. Red dots are the values calculated numerically from Eq. (15) and interpolate between the two limits.

two limits. In the short-time limit, it lies between the two limiting cases, while in the long-time limit it has a significantly lower value than both limits. In the short-time region shown in Fig. 5(d), the numerical calculation coincides with Eq. (30) (thick green line), and the MSD grows linearly with a slope that increases with α . At saturation, the MSD for $\alpha = 0.1$ equals $\sim 0.6d_0^2$, for $\alpha = 2$ equals $\sim 0.4d_0^2$, and for $\alpha = 10$, it approaches $\sim 0.2d_0^2$, indicating that the colloid motion is more localized when the electrostatic force is strong.

A distinct difference between the MSD for different α values is the characteristic time at which MSD saturates. This is the time it takes the colloid to explore its available space. Denoting τ_D as the time at which the MSD reaches half of its maximal value (the diffusion characteristic time), we obtain that in the $\alpha = 0$ case, $\tau_D = d_0^2 \ln 2/(2D_0)$ [see Eq. (22)], while in the $\alpha \rightarrow \infty$ limit, $\tau_D = k_B T \ln 2/(D_0 K) = d_0^2 \ln 2/(D_0 \alpha)$ [see Eq. (27)]. In Fig. 6, τ_D scaled by d_0^2/D_0 is shown as a function of α . Similar to D_{app} , the diffusion characteristic time τ_D interpolates between the two limits mentioned above, where the crossover occurs around $\alpha \sim 1$. The decrease of τ_D as a function of α , seen in Fig. 6, is attributed to two effects. First, as α increases, the colloid is more localized due to electrostatic forces and explores a smaller region, and second, its average diffusion coefficient, being further away from the walls, becomes larger.

E. Dependence of α on electrostatic properties

So far we have seen that the dynamics are determined by the value of α . Substituting the value of K derived in Eq. (7), we obtain

$$\alpha = \left(\frac{2\pi a d_0^2}{\epsilon_0 \epsilon k_B T} \right) \frac{2\sigma_c \sigma_w \cosh(\kappa_D d_0) + \sigma_c^2 + \sigma_w^2}{\sinh^2(\kappa_D d_0)}. \quad (34)$$

In an experimental setup, α can be controlled by changing the ionic strength (salt concentration, n), and consequently the Debye length, $\lambda_D \sim 1/\sqrt{n}$. The dependence of α on $\lambda_D = \kappa_D^{-1}$ is plotted in Fig. 7, for reasonable colloid and solvent param-

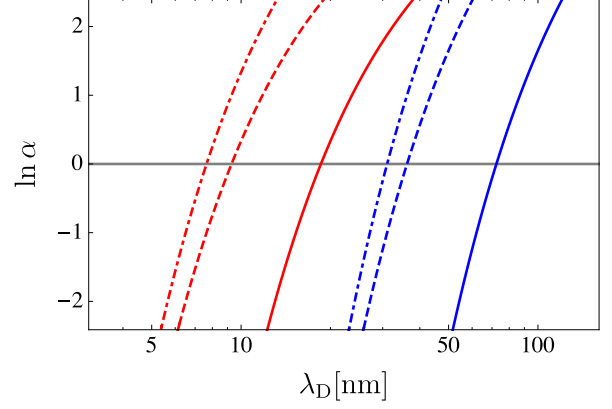


FIG. 7. The natural logarithm of the dimensionless parameter $\alpha = K d_0^2 / k_B T$, where K is given by Eq. (7), as a function of the screening length, λ_D , on a logarithmic scale. The system parameters are $L = 5 \mu\text{m}$, $\sigma_c = 0.003 e/\text{nm}^2$, $T = 300 \text{K}$, and $\epsilon = 80$. Blue lines are for $d_0 = 500 \text{nm}$ ($a = 2.0 \mu\text{m}$), and red lines are for $d_0 = 100 \text{nm}$ ($a = 2.4 \mu\text{m}$). Solid lines are for uncharged walls, $\sigma_w = 0$, dashed lines are for walls with surface charge density, $\sigma_w = \sigma_c$, and dot-dashed line are for $\sigma_w = 10\sigma_c$.

eters. As expected, α is large for large screening length and decreases towards zero as λ_D decreases.

As we have shown, $\alpha = 1$ signifies the crossover from a PCCD dominated motion to an electrostatically dominated one. For the range of parameters in Fig. 7, this crossover occurs roughly when $\lambda_D \sim d_0/10$. The screening length that corresponds to the crossover increases with d_0 , and for a fixed σ_c (σ_w), it decreases as σ_w (σ_c) increases.

V. SUMMARY AND DISCUSSION

We studied the dynamics of a charged colloid under restricted confinement of two charged surfaces. The combination of electrostatic and hydrodynamic forces exerted by the walls result in a unique behavior. This behavior can be quantified in terms of a dimensionless parameter α in Eq. (31) that determines the interplay between the electrostatic interaction and the position-dependent drag force. The parameter α is also given by Eq. (34), showing how the colloid motion, including its short-time behavior, Eq. (30), and long-time behavior (Figs. 5 and 6), depends on the geometry and electrostatic properties. In particular, α can be tuned by changing the screening length (Fig. 7) that is usually an easily controlled parameter in experiments. At small screening length (small α), the colloid moves slower than at larger screening length (large α). In addition, as λ_D is increased the colloid explores a smaller region in space throughout its motion. The two effects lead to a decrease in the diffusion characteristic time, τ_D , as λ_D is increased.

We note that the harmonic approximation of the interaction potential allows us to obtain analytical results. If we use the full interaction potential, Eq. (4), in the dynamical equation, we could not have expressed it in terms of a single parameter, α , as in Eq. (32). This harmonic approximation underestimates the strength of the interaction potential near the walls. However, as long as d_0 is of the order of the screen-

ing length, or smaller, the approximation is valid except for the regime very close to the wall where the interaction potential U diverges. This small region near the walls does not affect the MSD that integrates the motion throughout the entire space. Moreover, the divergence of U close to the wall is unphysical because at such close proximity the DH theory, Eq. (1), is no longer valid. For $d_0 \gg \lambda_D$, the following limiting expression should be used instead:

$$U(x) \approx \frac{2Q\sigma_w}{\varepsilon_0 \varepsilon \kappa_D^2 a} e^{-\kappa_D d_0} \cosh(\kappa_D x). \quad (35)$$

However, as in this limit the interaction potential is very small and can be ignored, there is no substantial difference in the MSD between the exact and approximated potentials.

We also note that, in our analysis, the effect of the ionic cloud on the diffusion coefficient of the charged colloid was neglected. In the free medium, the effect of the ionic cloud was calculated and turned out to be very small (of only a few percent) [25,26]. Since in a restricting confinement this effect was not fully investigated [18,32], it is not considered here for simplicity.

Although the above-mentioned calculations are approximated, we expect our results to qualitatively describe the Brownian motion of a charged colloid between confining charged walls. This should be tested in future experiments that will focus on very restricted confinement, as considered here.

ACKNOWLEDGMENTS

We would like to thank R. Adar for useful discussions. Y.A. is thankful for the support of the Clore Scholars Programme of the Clore Israel Foundation and the hospitality at Tokyo Metropolitan University, where part of this work has been conducted. S.K. acknowledges support by a Grant-in-Aid for Scientific Research (C) (Grants No. 18K03567 and No. 19K03765) from the Japan Society for the Promotion of Science, and support by a Grant-in-Aid for Scientific Research on Innovative Areas ‘‘Information Physics of Living Matters’’ (Grant No. 20H05538) from the Ministry of Education, Culture, Sports, Science and Technology of Japan. D.A. acknowledges support from the Israel Science Foundation (ISF) under Grant No. 213/19.

APPENDIX A: DERIVATION OF EQ. (4)

In the large sphere limit, the force acting on the colloid from the right wall is independent of that acting from the left wall, and vice versa. For each side, the force on the colloid is approximated by the Derjaguin approximation [22]

$$F(d) \approx 2\pi a \int_d^\infty dl \Pi(l), \quad (A1)$$

where Π is the force per unit area exerted on the colloid, if the colloid is considered as flat rather than spherical, and d is the distance between the colloid and the wall ($d = d_\ell$ for the left wall and $d = d_r$ for the right wall).

The electrostatic potential in the Derjaguin approximation can be calculated in a straightforward way. As it was performed multiple times for other geometries and boundary

conditions [22], we describe it only briefly here. Since the two sides of the colloid are decoupled, we start by solving the DH equation in Eq. (1) for a single wall, while assuming that the colloid is flat ($a \rightarrow \infty$). Denoting the distance from the left wall, without loss of generality, by ξ , the boundary conditions are $d\psi/d\xi|_{\xi=0} = -\sigma_w/(\varepsilon_0 \varepsilon)$ and $d\psi/d\xi|_{\xi=d} = \sigma_c/(\varepsilon_0 \varepsilon)$. Then the solution is

$$\psi(\xi; d) = \frac{\sigma_w \cosh[\kappa_D(d - \xi)] + \sigma_c \cosh(\kappa_D \xi)}{\varepsilon \varepsilon_0 \kappa_D \sinh(\kappa_D d)}. \quad (A2)$$

The DH approximation is valid when the electrostatic potential on the wall ($\xi = 0$) and on the colloid surface ($\xi = d$) is small compared to $k_B T/e$ [23]. This is satisfied when $\sigma_c, \sigma_w \ll e/(\ell_B \lambda_D)$ and $\sigma_c, \sigma_w \ll ed/(\ell_B \lambda_D^2)$, where $\ell_B = e^2/(4\pi \varepsilon_0 \varepsilon k_B T)$ is the Bjerrum length. When the colloid gets very close to the wall, $d \rightarrow 0$, the above Derjaguin approximation fails. However, as discussed in Sec. V, this regime does not affect our results.

One can show that the force per unit area, $\Pi(d)$, is independent of ξ and equals to [23,24]

$$\begin{aligned} \Pi(d) &= \frac{\varepsilon \varepsilon_0}{2} [-\psi'^2(\xi; d) + \kappa_D^2 \psi^2(\xi; d)] \\ &= -\frac{2\sigma_c \sigma_w \cosh(\kappa_D d) + \sigma_c^2 + \sigma_w^2}{2\varepsilon \varepsilon_0 \sinh^2(\kappa_D d)}, \end{aligned} \quad (A3)$$

where $\psi' = d\psi/d\xi$. Substituting Eq. (A3) into Eq. (A1), we obtain the force between the colloid and one surface. Integrating the force, we further get the interaction potential U_1 with a single wall, $U_1(d) = -\int_\delta^d dh F(h)$ where the lower cutoff δ is an arbitrary distance. The total interaction potential of the colloid, when taking into account the two walls, is $U(x) = U_1(d_0 + x) + U_1(d_0 - x)$. After some algebra, we obtain

$$\begin{aligned} U(x) &= \frac{\pi a}{\varepsilon \varepsilon_0 \kappa_D^2} \left[2\sigma_c \sigma_w \ln \left(\frac{\cosh(\kappa_D d_0) + \cosh(\kappa_D x)}{\cosh(\kappa_D d_0) - \cosh(\kappa_D x)} \right) \right. \\ &\quad \left. + (\sigma_c^2 + \sigma_w^2) \ln \left(\frac{\cosh(2\kappa_D d_0)}{\cosh(2\kappa_D d_0) - \cosh(2\kappa_D x)} \right) \right]. \end{aligned} \quad (A4)$$

We note that since $U(x)$ is constructed from integrating Π twice, the effective spring constant $K = U''|_{x=0}$ [see Eq. (6)] can be directly obtained from Π ,

$$K = 4\pi a \Pi(d_0). \quad (A5)$$

APPENDIX B: CHARGED WALLS WITH FIXED SURFACE ELECTROSTATIC POTENTIAL

Assuming that the walls have a fixed surface electrostatic potential, V , we repeat the calculation of Appendix A and Sec. II.

For the space between the left wall and the colloid, the boundary conditions are $\psi|_{\xi=0} = V$ and $d\psi/d\xi|_{\xi=d} = \sigma_c/(\varepsilon_0 \varepsilon)$. The solution to Eq. (1) is

$$\psi(\xi) = \frac{V \varepsilon_0 \varepsilon \kappa_D \cosh[\kappa_D(d - \xi)] + \sigma_c \sinh(\kappa_D \xi)}{\varepsilon \varepsilon_0 \kappa_D \cosh(\kappa_D d)}, \quad (B1)$$

and following a similar calculation as done in Appendix A, the total interaction potential is

$$U(x) = \frac{\pi a}{\varepsilon \varepsilon_0 \kappa_D^2} \left\{ [(V \varepsilon_0 \varepsilon \kappa_D)^2 - \sigma_c^2] \ln (\cosh[\kappa_D(d_0 + x)] \cosh[\kappa_D(d_0 - x)]) \right. \\ \left. - 4\sigma_c V \varepsilon \varepsilon_0 \kappa_D \left[\tan^{-1} \left(\tanh \frac{\kappa_D(d_0 + x)}{2} \right) + \tan^{-1} \left(\tanh \frac{\kappa_D(d_0 - x)}{2} \right) \right] \right\}. \quad (\text{B2})$$

Qualitatively, the behavior of U when varying V is similar to its behavior in Sec. II. The stability condition is

$$\delta > e^{-\kappa_D d_0} \quad \text{or} \quad \delta < -e^{\kappa_D d_0}, \quad (\text{B3})$$

where $\delta = V \varepsilon_0 \varepsilon \kappa_D / \sigma_c$. Unlike Sec. II, here the stability condition does not coincide with the condition that the walls repel the colloid at the midplane. The latter condition is

$$\delta > \frac{1}{e^{\kappa_D d_0} + \sqrt{1 + e^{2\kappa_D d_0}}} \quad \text{or} \quad \delta < \frac{1}{e^{\kappa_D d_0} - \sqrt{1 + e^{2\kappa_D d_0}}}. \quad (\text{B4})$$

If the stability condition of Eq. (B3) is satisfied, we can approximate the interaction potential around $x = 0$, to be $U \approx Kx^2/2$, with the effective spring constant

$$K = \left(\frac{2\pi a}{\varepsilon \varepsilon_0} \right) \frac{2\sigma_c V \varepsilon \varepsilon_0 \kappa_D \sinh(\kappa_D d_0) + (V \varepsilon \varepsilon_0 \kappa_D)^2 - \sigma_c^2}{\cosh^2(\kappa_D d_0)}. \quad (\text{B5})$$

As shown in Sec. IV D, the value of K determines the type of colloid diffusion. For a fixed σ_c , K grows as V is increased, and decays to zero for $\kappa_D d_0 \gg 1$.

-
- [1] P. S. Burada, P. Hänggi, F. Marchesoni, G. Schmid, and P. Talkner, *Chem. Phys. Chem.* **10**, 45 (2009).
- [2] R. Phillips, J. Kondev, J. Theriot, and H. Garcia, *Physical Biology of the Cell* (Garland Science, London, 2012).
- [3] T. M. Squires and S. R. Quake, *Rev. Mod. Phys.* **77**, 977 (2005).
- [4] M. Krishnan, N. Mojarad, P. Kukura, and V. Sandoghdar, *Nature (London)* **467**, 692 (2010).
- [5] F. Ruggeri and M. Krishnan, *Phys. Rev. E* **96**, 062406 (2017).
- [6] H. Brenner, *Chem. Eng. Sci.* **16**, 242 (1961).
- [7] A. J. Goldman, R. G. Cox, and H. Brenner, *Chem. Eng. Sci.* **22**, 637 (1967).
- [8] P. Ganatos, S. Weinbaum, and R. Pfeffer, *J. Fluid Mech.* **99**, 739 (1980).
- [9] P. Ganatos, R. Pfeffer, and S. Weinbaum, *J. Fluid Mech.* **99**, 755 (1980).
- [10] K. H. Lan, N. Ostrowsky, and D. Sornette, *Phys. Rev. Lett.* **57**, 17 (1986).
- [11] L. Lobry and N. Ostrowsky, *Phys. Rev. B* **53**, 12050 (1996).
- [12] M. Hosoda, K. Sakai, and K. Takagi, *Phys. Rev. E* **58**, 6275 (1998).
- [13] M. A. Bevan and D. C. Prieve, *J. Chem. Phys.* **113**, 1228 (2000).
- [14] P. Lançon, G. Batrouni, L. Lobry, and N. Ostrowsky, *Physica A* **304**, 65 (2002).
- [15] E. R. Dufresne, D. Altman, and D. G. Grier, *Europhys. Lett.* **53**, 264 (2001).
- [16] P. Huang and K. S. Breuer, *Phys. Rev. E* **76**, 046307 (2007).
- [17] G. M. Kepler and S. Fraden, *Langmuir* **10**, 2501 (1994).
- [18] S. L. Eichmann, S. G. Anekal, and M. A. Bevan, *Langmuir* **24**, 714 (2008).
- [19] S. Fringes, F. Holzner, and A. W. Knoll, *Beilstein J. Nanotechnol.* **9**, 301 (2018).
- [20] M. I. M. Feitosa and O. N. Mesquita, *Phys. Rev. A* **44**, 6677 (1991).
- [21] N. A. Frej and D. C. Prieve, *J. Chem. Phys.* **98**, 7552 (1993).
- [22] J. Israelachvili, *Intermolecular and Surface Forces*, 3rd ed. (Academic, New York, 2011).
- [23] T. Markovich, D. Andelman, and R. Podgornik, in *Handbook of Lipid Membranes: Molecular, Functional, and Materials Aspects*, edited by C. Safinya and J. Raedler (CRC Press, Taylor & Francis Group, 2021), Chap. 6.
- [24] V. A. Parsegian and D. Gingell, *Biophys. J.* **12**, 1192 (1972).
- [25] H. Ohshima, T. W. Healy, L. R. White, and R. W. O'Brien, *J. Chem. Soc., Faraday Trans. 2* **80**, 1299 (1984).
- [26] G. A. Schumacher and T. G. M. van de Ven, *Faraday Discuss.* **83**, 75 (1987).
- [27] L. P. Faucheux and A. J. Libchaber, *Phys. Rev. E* **49**, 5158 (1994).
- [28] T. Benesch, S. Yiacoumi, and C. Tsouris, *Phys. Rev. E* **68**, 021401 (2003).
- [29] B. Lin, J. Yu, and S. A. Rice, *Phys. Rev. E* **62**, 3909 (2000).
- [30] A. W. C. Lau and T. C. Lubensky, *Phys. Rev. E* **76**, 011123 (2007).
- [31] H. Risken, *The Fokker-Planck Equation* (Springer, Berlin, Heidelberg, 1996).
- [32] B. Chun and A. J. C. Ladd, *J. Colloid Interface Sci.* **274**, 687 (2004).